Ab initio stability prediction of β titanium and α and ω precipitates in β titanium matrix for titanium alloys using density functional theory and micromechanics

Akio Ishii*

** Department of Mechanical Science and Bioengineering, Osaka University, 1-3, Machikaneyama, Toyonaka, Osaka, 560-8531, Japan*

Abstract

β titanium alloys have a wide range of applications, including in aerospace and transport. The β phase is stable only at high temperatures, and the phase stability can be improved by adding stabilizers. However, the β-phase-stabilization effects of β stabilizers have not yet been clearly elucidated. Here, we report the *ab initio* prediction of the energetic phase stability of β titanium alloys with Mo, V, W, Nb, and Ta as additive β stabilizer elements. The stability is predicted using a combination of atomistic simulation via density functional theory and continuum micromechanics (Eshelby's ellipsoidal inclusion analysis). In particular, we consider the heterogeneity of the secondary ω and α phases (precipitation) in the β matrix. All β stabilizer species led to a significant energetic and elastic stabilization of the β phase. Mo and W additives turned the β phase energetically the most stable and secondary ω and α precipitates may hardly nucleate in β phase in high concentrate condition. Although V, Nb, and Ta additives stabilized the β phase significantly, the β phase remained metastable. Regarding the morphology of these secondary phases, V helped α precipitation and Ta helped ω precipitation. The possibility of a coexistence of ω and α in the β matrix was suggested for Nb addition. The strain fields around the precipitates were also investigated and the results suggested that α precipitates cause a large residual strain around it though ω precipitates do not.

Keywords: Titanium alloy, Eshelby's ellipsoidal inclusion, Atomistic simulation, Density functional theory

---

*Corresponding author

Email address: ishii@me.es.osaka-u.ac.jp (Akio Ishii)

1. Introduction

Titanium alloys are promising materials for applications in various fields—including aerospace, transportation, and implants—owing to their light weight and good biocompatibility [1, 2]. Pure titanium has three phases with different atomic structures: hexagonal close-packed (HCP) α phase, body-centered cubic (BCC) β phase, and hexagonal ω phase. β titanium alloys are considered particularly suitable materials for the aforementioned applications because of their high strength and corrosion resistance [3–5]. For pure titanium, previous theoretical and experimental studies have revealed that the α phase is stable at room temperature and ordinary pressure, the ω phase is stable at low temperature and high pressure, and the β phase is stable at only high temperatures [6]. In this context, alloying is necessary to improve the stability of the β phase.

β titanium alloys primarily consist of three types of additive elements: β stabilizers (Mo, V, W, Nb, Ta, Fe, Cr, Cu, etc.), α stabilizers (Al, O, N), and elements that construct the master alloy to reduce the high melting point of titanium [3]. High-performance on-demand β titanium alloys have been developed by varying the species and fractions of the three types of additives [2, 5, 7]. Several theoretical approaches have been proposed for the design of titanium alloys (for example, the *d* electron alloys designing) [8, 9]. Nonetheless, alloy design is challenging and time-consuming because it usually depends on empirical trial-and-error iterative experiments. Hence, quantitative analyses to help design β titanium alloys are still insufficient. For example, the β-phase-stabilization effects of β stabilizers and their effects on the precipitation of secondary ω or α phases in the β matrix (because β phase is usually stable) [10–14] are not yet clearly elucidated.

However, with the development of computers, $ab\ initio$ atomistic simulations of materials using density functional theory (DFT) has become common and computationally aided material design based on atomistic simulation is expected. For example, Materials Project [15, 16], which provides access to big data on material properties and atomic structures calculated using DFT atomistic simulations, can help in practical material design. Moreover, alloy designs based on DFT atomistic simulations have been investigated [17]. In this study, we used a combination of DFT atomistic simulations and continuum micromechanics aim to computationally design titanium alloys. We predicted the phase stability of β titanium alloys energetically for the additive elements Mo, V, W, Nb and Ta, which do not cause the compound [3], considering the heterogeneity of the secondary ω and α phases (precipitation) in β matrix. Previous investigations on the phase stabilities of titanium alloys using DFT atomistic simulations [18–22], have usually focused on the analysis of *homogeneous* atomic structures of each phase due to the limitations of DFT atomistic simulations (such as high computational cost). To the best of our knowledge, an $ab\ initio$ analysis of the phase stability of titanium alloys that considers the *heterogeneous* precipitation of the secondary phase has not yet been conducted.

In a previous study, we proposed an $ab\ initio$ parameter-free multiscale analysis combining Eshelby's ellipsoidal inclusion analysis (micromechanics) and DFT atomistic simulation. Therein, we successfully predicted the morphology of Zr hydride precipitates and cracks in the Zr (HCP structure) matrix as well as the morphology and stability of the B19' phase in the B2 matrix of TiNi shape memory alloys [23–26]. In this study, we applied our method to predict the phase stability of titanium alloys by considering the heterogeneity of the secondary phases. For pure titanium and titanium alloys with the aforementioned additive elements, we first calculated the potential energy, the elastic constants of the β, ω, and α phases, and the eigenstrains for $\beta-\omega$ and $\omega-\alpha$ phase transformations using DFT atomistic simulations. Thereafter, the phase stability in the limitation of homogeneity is discussed. Next, for cases with possible nucleation of the ω or α secondary phase in the β matrix (β is metastable), we employed Eshelby's ellipsoidal inclusion analysis to investigate the stability of the ω or α precipitates using the calculated elastic constants of each phase and eigenstrains of the phase transformations.

2. DFT atomistic simulation

2.1. Atomistic models and calculation setting

The atomic models used in the DFT atomistic simulation are shown in Fig. 1.We employed two sets of atomic models, I and II, to compute the eigenstrains of the $\beta-\omega$ and $\omega-\alpha$ phase transformations. In set I, the atomic models of the BCC structure, β titanium, were prepared with a lattice constant of 0.325 nm. This model included 6 Ti atoms in a unit cell. To reproduce $\beta-\omega$ phase transformation, the directions of the edge vectors of the supercell, $\boldsymbol{h_1}$, $\boldsymbol{h_2}$, and $\boldsymbol{h_3}$, were set to $[111]_\beta$, $[01\bar{1}]_\beta$, and $[1\bar{1}0]_\beta$ respectively. The atoms in the (111) layers (green and blue in Fig. 1) were shuffled along the direction of black arrows. The atomic structure as well as the size and shape of the supercell [27] were optimized to obtain a hexagonal ω atomic structure. The orientation relationships between β and ω were $[111]_\beta \parallel [0001]_\omega$, $[11\bar{2}]_\beta \parallel [1\bar{1}00]_\omega$ and $[1\bar{1}0]_\beta \parallel [11\bar{2}0]_\omega$, which are consistent with experimental observations [10, 27].

In set II, to reproduce $\omega-\alpha$ phase transformation, the edge vectors of the supercell of the prepared ω atomic model (of set I) were changed to the orthogonal $[0001]_\omega$, $[1\bar{1}00]_\omega$, and $[11\bar{2}0]_\omega$; the atomic model was reconstructed as a 12-atom unit cell. Crystallographically, ω titanium has 2 layers stacked along $[11\bar{2}0]_\omega$ (ABAB…), as shown in Fig. 1. In accordance with the suggestion by Silcock et al. [18, 28], the atoms in each layer were shuffled along the direction of the black arrows in the figure. The atomic structure as well as the size and shape of the supercell were optimized to obtain the HCP α atomic model. The orientation relationships between β and α were $[111]_\beta \parallel [11\bar{2}0]_\alpha$, $[11\bar{2}]_\beta \parallel [1\bar{1}00]_\alpha$, and $[1\bar{1}0]_\beta \parallel [1\bar{1}00]_\alpha$, which are consistent with experimental observations [10]. Trinkle et al. have suggested another shuffling pathway for the $\omega-\alpha$ phase transformation [6,

18]. However, we employed the pathway suggested by Silcock et al. because it results in a smaller $\omega-\alpha$ eigenstrain and is elastically favorable when the heterogeneity of the secondary α phase is considered.

Next, we prepared atomic models of titanium alloys Ti_5X_1 (where X is an additive element) by replacing the Ti atoms marked X with Mo, V, W, Nb, and Ta atoms, as shown in Fig. 1. We calculated the potential energies and elastic constants for all the phases of all the additive elements using these atomic models. Using the cell matrix $\boldsymbol{H} = [\boldsymbol{h_1}\ \boldsymbol{h_2}\ \boldsymbol{h_3}]$ constructed using the edge vectors of the optimized atomic structures, the eigenstrains ϵ_{ij} for the phase transformation can be derived in the form of Green strain as

$$\epsilon_{ij} = \frac{1}{2}(\boldsymbol{J}^{\mathbf{T}}\boldsymbol{J} - \boldsymbol{I}), \tag{1}$$

where $\boldsymbol{J}^{\mathbf{T}} = \boldsymbol{H}_{\mathbf{fin}}(\boldsymbol{H}_{\mathbf{ini}})^{-1}$ denotes the deformation tensor [23, 25, 26]. $\boldsymbol{H}_{\mathbf{ini}}$ and $\boldsymbol{H}_{\mathbf{fin}}$ denote the cell matrices of the atomic structure before and after phase transformation, respectively.

The Vienna Ab initio Simulation Package [29] was used for the DFT atomistic simulations (including the optimization mentioned above). The electron-ion interaction in DFT is described using the projector-augmented wave method [30]. The exchange-correlation between electrons was treated using the Perdew–Burke–Ernzerhof generalized gradient approximation [31]. The energy cutoff for the plane-wave basis set was set to 300 eV. The energy convergence criteria for the electronic and ionic structure relaxations were set to 1.0×10^{-8} and 1.0×10^{-4} eV, respectively. A $6 \times 6 \times 12$ k-point mesh was used for the atomic models in set I, and a $12 \times 4 \times 12$ k-point mesh was used for the atomic models in set II. The β and ω atomic models of set I and the HCP atomic model of set II were used to calculate the potential energies and elastic constants. The finite difference approach was used to calculate the elastic constants. The entropy effect with respect to the temperature was not considered because of the calculation cost.

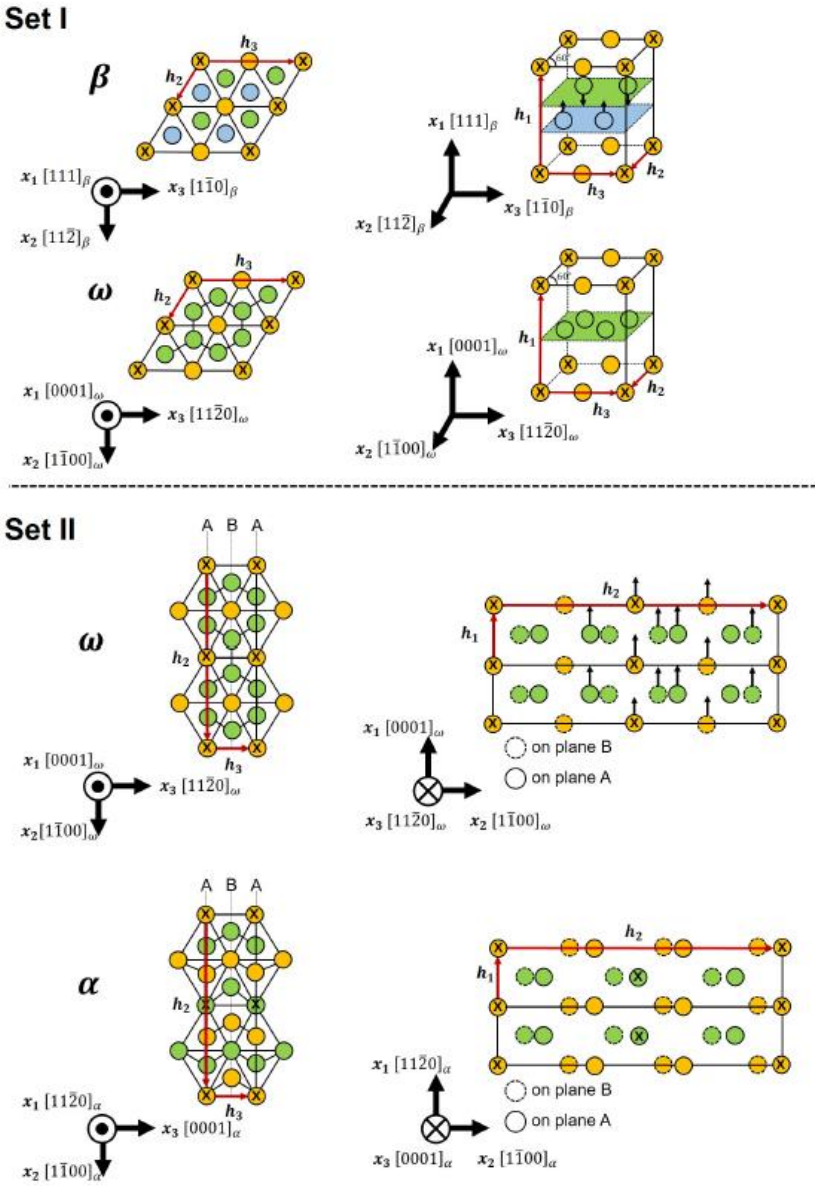

Figure 1: Atomic models of β, ω and α titanium used for DFT atomistic simulation. The circles indicate the positions of atoms. β and ω atomic models (supercell) in set I, containing 6 atoms, were used to calculate the eigenstrain of the $\beta-\omega$ phase transformation. ω and α atomic models in set II, containing 12 atoms, were used to calculate the eigenstrain of the $\omega-\alpha$ phase transformation. The colors of the atoms indicate the atoms belong to same $(111)_\beta$ plane, corresponding to $(0001)_\omega$ and $(11\bar{2}0)_\alpha$ plane. The black arrows indicate the direction of the atomic shuffling for the $\beta-\omega$ (set I) and $\omega-\alpha$ (set II) phase transformations. The red arrows in the figures indicate the edge vectors $\boldsymbol{h_1}$, $\boldsymbol{h_2}$ and $\boldsymbol{h_3}$ of the supercells of each atomic model. The black solid lines are included as a guide to clarify the crystallography of each atomic model. The Ti atoms marked X were replaced with Mo, V, W, Nb, and Ta to construct the atomic models of titanium alloys Ti_5X_1.

2.2. Results and discussion

Table 1 lists the calculated differences in the potential energies of the ω and α phases from that of the β phase for each additive element. For pure Ti, although the energy difference between ω and α is not large, the ω phase is the most stable with the lowest energy. The energy of the β phase is the highest, and thus, β is energetically unstable. However, with the addition of β stabilizer elements, the energy differences generally become significantly small. In particular, with Mo and W addition, the β phase becomes the most stable. Although the concentration of the additive elements is considerably high compared with the experimental alloy composition due to the limitation of DFT atomistic simulation, this suggests Mo and W not strongly stabilize β. Moreover, the addition of V, Nb, and Ta significantly decreases the energy difference between β and ω as well as between β and α. However, the β phase remains metastable, suggesting that the nucleation of secondary ω or α occurs and the effect of stabilization of them is relatively weak in these additives.

Table 2 lists the calculated elastic constants of the β, ω, and α phases for each additive species in the coordinate system $[111]_\beta - [11\bar{2}]_\beta - [1\bar{1}0]_\beta$. For pure Ti, C_{1212} and C_{3131} are considerably small (almost zero). If the coordinate system is changed to the conventional $[100]_\beta - [010]_\beta - [001]_\beta$, we find $C_{1111} - C_{1112} < 0$. The well-known Born criteria for the elastic instability of the BCC structure [32] indicate that the pure β titanium phase is elastically unstable. However, the addition of β stabilizer elements neutralizes this instability; C_{1212} and C_{3131} become large, and $C_{1111} - C_{1112} > 0$ in the conventional $[100]_\beta - [010]_\beta - [001]_\beta$ coordinate system. This indicates that the β stabilizer elements stabilize the β phase both energetically and elastically. We also investigated the elastic instabilities of ω and α using the Born criteria for hexagonal structures [33]. The results indicated that the ω and α phases are elastically stable in all cases. The β stabilizers investigated in this study generally increased the elastic constants for all phases. Hence, these species may not be effective for designing titanium alloys for biomaterials whose elastic constants must be as low as those of human bones.

Table 3 lists the calculated eigenstrains of the $\beta - \omega$ and $\omega - \alpha$ phase transformations for each additive species in the coordinate system $[111]_\beta - [11\bar{2}]_\beta - [1\bar{1}0]_\beta$. The eigenstrains of pure Ti are small. However, the eigenstrains of titanium alloys—ϵ_{11} for $\omega - \alpha$ ($[111]_\beta$ normal strain) in particular—are large. The $\beta - \omega$ phase transformation comprises shear components apart from normal components for the titanium alloys. We confirmed that the shear components originate from the additive-induced distortion of the β phase from the original BCC structure. This result suggests that alloying increases the residual strain (or stress) caused by the secondary ω and α precipitates in the β matrix. The energies of the α and ω phases are lower than that of the β phase from DFT calculation in Table 1. However, in the case of heterogeneously nucleated α and ω in the β matrix,

the energy hierarchy may change elastically owing to the large eigenstrain. Hence, the elastic energy increments due to the heterogeneity must be considered. The next section details Eshelby's ellipsoidal inclusion analysis for the V, Nb, and Ta cases wherein the β phase is metastable. Therein, the stability is discussed while considering the effect of heterogeneity of the α and ω precipitates in the β matrix.

Table 1: Potential energy differences of ω and α titanium from β titanium for each additive species calculated using DFT atomistic simulation. The potential energies are in eV/atom.

	ω	α
Pure Ti	-0.1187	-0.1105
Ti_5Mo_1	0.0879	0.0286
Ti_5V_1	0.0025	-0.0135
Ti_5W_1	0.0475	0.0229
Ti_5Nb_1	-0.0046	-0.0090
Ti_5Ta_1	-0.0459	-0.0272

Table 2: Elastic constants of β, ω, and α titanium for each additive species calculated using DFT atomistic simulation. Note that $C_{ijkl} = C_{jikl} = C_{ijlk} = C_{klij}$. The values of C_{ijkl} that are not listed here are all zero. The elastic constants are in GPa. The coordinate system is $[111]_\beta - [11\bar{2}]_\beta - [1\bar{1}0]_\beta$.

	Pure Ti	Ti_5Mo_1	Ti_5V_1	Ti_5W_1	Ti_5Nb_1	Ti_5Ta_1
β						
C_{1111}	164	194	189	209	197	201
C_{2222}	144	187	164	201	176	181
C_{3333}	144	191	168	202	180	182
C_{1122}	77	90	82	91	80	80
C_{1133}	77	80	76	83	73	76
C_{2233}	98	109	111	104	102	99
C_{2323}	25	32	26	39	31	32
C_{3131}	8	36	31	37	28	26
C_{1212}	5	51	42	52	40	36
C_{1123}	0	-8	-5	-6	-6	-4
C_{1131}	0	0	0	0	5	7

C_{1112}	0	0	0	0	0	4
C_{2223}	0	9	0	10	8	8
C_{2231}	0	0	0	-6	-6	-7
C_{2212}	25	-6	0	0	0	8
C_{3323}	0	-6	0	-8	-5	-8
C_{3331}	0	-8	-5	-5	-5	-4
C_{3312}	-25	0	5	-7	-7	-14
C_{2331}	-25	0	0	-4	-4	-9
C_{3112}	0	-13	-9	-14	-10	-9
ω						
C_{1111}	252	274	261	295	251	262
C_{2222}	201	201	197	216	182	193
C_{3333}	200	188	200	209	181	194
C_{1122}	51	72	63	78	70	70
C_{1133}	51	62	56	65	64	64
C_{2233}	81	117	104	114	114	110
C_{2323}	60	26	39	36	30	41
C_{3131}	56	21	44	29	37	44
C_{1212}	56	11	43	32	34	45
α						
C_{1111}	170	161	140	164	139	139
C_{2222}	170	180	174	189	166	181
C_{3333}	195	161	174	175	169	178
C_{1122}	90	94	104	100	103	105
C_{1133}	75	118	118	124	121	126
C_{2233}	75	88	72	87	75	66
C_{2323}	43	22	59	33	53	59
C_{3131}	43	30	37	35	35	38
C_{1212}	40	54	60	63	63	62

Table 3: Eigenstrains for the β to ω and ω to α phase transformations of titanium for each additive species calculated using DFT atomistic simulation. Note that $\epsilon_{ij} = \epsilon_{ji}$. The coordinate system is $[111]_\beta - [11\bar{2}]_\beta - [1\bar{1}0]_\beta$.

	Pure Ti	Ti_5Mo_1	Ti_5V_1	Ti_5W_1	Ti_5Nb_1	Ti_5Ta_1
β to ω						
ϵ_{11}	0.0057	-0.0325	-0.0196	-0.0263	-0.0100	-0.0054
ϵ_{22}	-0.0063	0.0417	0.0278	0.0324	0.0233	0.0189
ϵ_{33}	-0.0055	-0.0032	-0.0070	-0.0049	-0.0070	-0.0100
ϵ_{23}	0.0	-0.0389	-0.0301	-0.0322	-0.0262	-0.0249
ϵ_{31}	0.0	-0.0552	-0.0568	-0.0550	-0.0531	-0.0538
ϵ_{12}	0.0	-0.0319	-0.0328	-0.0318	-0.0307	-0.0311
ω to α						
ϵ_{11}	0.0377	0.1988	0.1741	0.2107	0.1868	0.1668
ϵ_{22}	-0.0364	-0.1160	-0.0863	-0.1133	-0.0970	-0.0891
ϵ_{33}	0.0166	-0.0271	-0.0394	-0.0357	-0.0433	-0.0360
ϵ_{23}	0.0	0.0	0.0	0.0	0.0	0.0
ϵ_{31}	0.0	0.0	0.0	0.0	0.0	0.0
ϵ_{12}	0.0	0.0	0.0	0.0	0.0	0.0

3. Eshelby's ellipsoidal inclusion analysis

3.1 Methodlogy

As mentioned in the previous section, the ω or α precipitates usually nucleate heterogeneously in the β matrix, and accounting for the effect of heterogeneity in conventional DFT calculations is usually difficult. In this study, we used a micromechanics approach—Eshelby's ellipsoidal inclusion analysis—to account for the heterogeneity of ω and α precipitates in the β matrix [23–26]. In micromechanics, the original strain-free shape of the secondary phase is described using the eigenstrain, whereas the shape elastically deformed due to heterogeneity is described as the total strain (the original zero-strain shape is defined as the shape of the matrix) [34]. If we consider the ω and α precipitates, as an ellipsoidal inclusion ($\frac{x_1^2}{a_1^2}+\frac{x_2^2}{a_2^2}+\frac{x_3^2}{a_3^2}=1$; $\boldsymbol{x}=[x_1;x_2;x_3]$ indicates the position inside the β matrix and a_i $(i=1,2,3)$ is half axis of ellipsoid in each direction) [35, 36], and the eigenstrains are uniformly distributed in the inclusion, the total strains and eigenstrains of the inclusion, $\varepsilon_{ij}^{\mathrm{inc}}$ and $\epsilon_{ij}^{\mathrm{inc}}$, are linearly connected with Eshelby's tensor, S_{klmn}, using Einstein summation convention,

$$\varepsilon_{kl}^{\mathrm{inc}} = S_{klmn}\epsilon_{mn}^{\mathrm{inc}}, \tag{2}$$

The general form of Eshelby's tensor for an anisotropic matrix and an inclusion is derived as follows [34, 37]:

$$S_{klmn} = \frac{1}{8\pi} C_{pqmn} \int_{-1}^{1} d\zeta_3 \int_0^{2\pi} \left(\frac{\xi_l \xi_q N_{kp}(\xi_1,\xi_2,\xi_3) + \xi_k \xi_q N_{lp}(\xi_1,\xi_2,\xi_3)}{D(\xi_1,\xi_2,\xi_3)} \right) d\theta, \tag{3}$$

where

$$D(\xi_1,\xi_2,\xi_3) = P_{pqr}\left(C_{pj1l}\xi_j\xi_l\right)\left(C_{qm2n}\xi_m\xi_n\right)\left(C_{rs3t}\xi_s\xi_t\right),$$

and

$$N_{km}(\xi_1,\xi_2,\xi_3) = \frac{1}{2} P_{kst} P_{mnr}\left(C_{sjnl}\xi_j\xi_l\right)\left(C_{turv}\xi_u\xi_v\right),$$

which correspond to the determinant and cofactor of $K_{km} = C_{klmn}^{\mathrm{mat}}\xi_l\xi_n$, respectively. P_{pqr} denotes the permutation tensor. Using ζ_3 and θ, $[\xi_1;\ \xi_2;\ \xi_3]$ can be expressed as

$$\begin{bmatrix} \xi_1 \\ \xi_2 \\ \xi_3 \end{bmatrix} = \begin{bmatrix} \frac{\sqrt{1-\zeta_3^2}\cos\theta}{a_1} \\ \frac{\sqrt{1-\zeta_3^2}\sin\theta}{a_2} \\ \frac{\zeta_3}{a_3} \end{bmatrix}.$$

In general, the distributed total strain $\varepsilon_{kl}(\boldsymbol{x})$ and eigenstrains $\epsilon_{kl}(\boldsymbol{x})$ lead to a distribution of the internal stress $\sigma_{ij}(\boldsymbol{x})$ [34]:

$$\sigma_{ij}(\boldsymbol{x}) = C_{ijkl}\big(\varepsilon_{kl}(\boldsymbol{x}) - \epsilon_{kl}(\boldsymbol{x})\big). \quad (4)$$

Using this equation, Eshelby's ``equivalent inclusion theory'' for ellipsoidal inclusion describes the relationship between the elastic constants of the matrix C_{ijkl}, that of the inclusion $\tilde{C}_{ijkl}$, and the fictitious eigenstrains $\tilde{\epsilon}_{mn}$ [34, 36],

$$\tilde{C}_{ijkl}\big(S_{klmn}\tilde{\epsilon}_{mn} + \varepsilon^{\mathrm{ex}}_{kl} - \epsilon^{\mathrm{inc}}_{kl}\ \big) = C_{ijkl}(S_{klmn}\tilde{\epsilon}_{mn} + \varepsilon^{\mathrm{ex}}_{kl} - \tilde{\epsilon}_{kl}) \quad (5)$$

where $\varepsilon^{\mathrm{ex}}_{kl}$ is the elastic strain of the matrix due to the external stress $\sigma^{\mathrm{ex}}_{ij}$. This equation replaces the inhomogeneity of the elastic constants with additional eigenstrains $\tilde{\epsilon}_{mn}$. The left and right-hand sides of this equation are derived from equation (4) for the real and fictitious inclusions, respectively. The total strain term is described using fictitious eigenstrains $\tilde{\epsilon}_{mn}$ as $\varepsilon^{\mathrm{inc}}_{kl} = S_{klmn}\tilde{\epsilon}_{mn}$. Solving these simultaneous equations for $\tilde{\epsilon}_{mn}$, the elastic energy increment ΔE^{het} (per unit volume of inclusion) due to the inclusion in the matrix under the external stress $\sigma^{\mathrm{ex}}_{ij}$ condition can be expressed as follows [34]:

$$\Delta E^{\mathrm{het}} = -\frac{1}{2}\sigma^{\mathrm{inc}}_{ij}\epsilon^{\mathrm{inc}}_{ij} - \sigma^{\mathrm{ex}}_{ij}\epsilon^{\mathrm{inc}}_{ij} - \frac{1}{2}\sigma^{\mathrm{ex}}_{ij}\big(\tilde{\epsilon}_{ij} - \epsilon^{\mathrm{inc}}_{ij}\big), \quad (6)$$

where $\sigma^{\mathrm{inc}}_{ij}$ is the internal stress of the ellipsoidal inclusion derived from equations (4). Considering the inhomogeneity between β, ω and α and the anisotropy of the elastic constants, we numerically calculated S_{klmn} and then determined ΔE^{het} using the above equations. S_{klmn} depends on the morphology of the inclusion. Hence, the minimum elastic energy increment $\Delta E^{\mathrm{het}}_{\mathrm{min}}$ was determined by changing the shape and orientation of the precipitates. The total energy change from the β matrix, $\Delta E_{\mathrm{total}}$ (per atom unit), was then determined to discuss the stability,

$$\Delta E_{\mathrm{total}} = \Delta E_{\mathrm{DFT}} + \Delta E^{\mathrm{het}}_{\mathrm{min}} V_{\mathrm{atom}}. \quad (7)$$

ΔE_{DFT} denotes the energy difference from the β phase listed in Table 1 and V_{atom} denotes the average atomic volume of the DFT supercell of β titanium. The chemical interfacial energy was not considered in this study because the sizes of the ω or α precipitates are generally large in experimental observations [10, 14]. We believe that, on a large scale, the area-dependent chemical interfacial energy is sufficiently small compared to the volume-dependent elastic energy and ΔE_{DFT}

in the above equation.

Once stable ω or α precipitates for a certain additive species were confirmed, we calculated the strain field around the precipitates [26, 38] because the existence of a strain (or stress) field is related to the precipitation strengthening of titanium alloys, and is important to design the mechanical property of alloys [14]. First, we numerically calculated the gradient of the displacement $\frac{\partial u_i}{\partial x_j}$ at a certain position $\boldsymbol{x}$ in the matrix due to the ellipsoidal inclusion with uniform eigenstrains as follows:

$$\frac{\partial u_i}{\partial x_j} = C_{klmn}\tilde{\epsilon}_{mn}\int_{-1}^{1} d\zeta_3 \int_0^{2\pi}\left(\frac{\xi_j\xi_l N_{ik}(\xi_1,\xi_2,\xi_3)}{D(\xi_1,\xi_2,\xi_3)}\left(\frac{1}{4\pi}U(\boldsymbol{x}\cdot\boldsymbol{\xi}-1)-\frac{1}{2\pi\tilde{x}}\delta(\boldsymbol{x}\cdot\boldsymbol{\xi}-1)\right)\right)d\theta, \quad (8)$$

where

$$U(x)=\begin{cases}1 & (x\le 0)\\ 0 & (x>0)\end{cases},$$

$$\delta(x)=\begin{cases}1 & (x=0)\\ 0 & (otherwise)\end{cases}.$$

The step function $U(x)$ and the delta function $\delta(x)$ limit the range of integration on the right-hand side to $\boldsymbol{x}\cdot\boldsymbol{\xi}<1$ and $\boldsymbol{x}\cdot\boldsymbol{\xi}=1$ for the first and second terms, respectively, and $\tilde{x}=\sqrt{\left(\frac{x_1}{a_1}\right)^2+\left(\frac{x_2}{a_2}\right)^2+\left(\frac{x_3}{a_3}\right)^2}$. Note the center of the inclusion is defined as $\boldsymbol{x}=[0;\ 0;\ 0]$. Next, using above equation (8) and the following relationship

$$\varepsilon_{ij}(\boldsymbol{x})=\frac{1}{2}\left(\frac{\partial u_i}{\partial x_j}+\frac{\partial u_j}{\partial x_i}\right),$$

the total strain distribution was derived. In addition, the stress distribution can be derived using equation (4). Note the position $\boldsymbol{x}$ can be both the inside and outside of the inclusion in the matrix and the above calculation gives $\varepsilon_{ij}(\boldsymbol{x})=\varepsilon_{ij}^{\mathrm{inc}}$ for the position $\boldsymbol{x}$ inside the ellipsoidal inclusion because $\boldsymbol{x}$ is always satisfied $\boldsymbol{x}\cdot\boldsymbol{\xi}<1$ during integration.

For the detailed calculation setting, we calculated $\Delta E_{\mathrm{total}}$ of the ω and α precipitates for the V, Nb, and Ta additive elements (which have negative ΔE_{DFT} values) using the elastic constants and eigenstrains listed in Table 2 and 3. The eigenstrains ($\epsilon_{ij}^{\mathrm{inc}}$) of the β to α transformation can be approximated via a simple addition of the eigenstrains of the β to ω and ω to α transformations listed in Table 3, referring to the order of transformation β to ω to α, which is usually observed in experiments [10–14]. Because the eigenstrain value of the $\beta-\omega$ phase transformation (Table 3) is

generally smaller than that of $\omega-\alpha$, we believe that this approximation (the addition of eigenstrains) is reasonable.

For simplicity, the precipitates are considered as needle or disk-shaped ellipsoidal inclusions; such shapes are usually stable precipitates [10, 14, 22]. Analytically, the disk and needle are shapes with extremely long and short half axes of inclusion (e.g., $a_1 = a_2$ and $a_3/a_1 \to 0$ for disk, $a_3/a_1 \to \infty$ for needle) [34, 39]. However, owing to the limitations of numerical calculations, we consider the $(a_1; a_2; a_3) = (20; 20; 1)$ and $(a_1; a_2; a_3) = (1; 1; 20)$ ellipsoids as disk and needle inclusions, respectively. For the orientations of the disk and needle-shaped inclusions, we describe the elastic constants and eigenstrains in the coordinate system $\boldsymbol{x}'$ of the rotated disk and needle inclusions using the following rotation matrix:

$$R_{ij} = \begin{bmatrix} \cos\psi & 0 & -\sin\psi \\ 0 & 1 & 0 \\ \sin\psi & 0 & \cos\psi \end{bmatrix} \times \begin{bmatrix} \cos\phi & \sin\phi & 0 \\ -\sin\phi & \cos\phi & 0 \\ 0 & 0 & 1 \end{bmatrix}$$
$$= \begin{bmatrix} \cos\psi\cos\phi & \cos\psi\sin\phi & -\sin\psi \\ -\sin\phi & \cos\phi & 0 \\ \sin\psi\cos\phi & \sin\psi\sin\phi & \cos\psi \end{bmatrix} \quad (9)$$

The normal direction of the disk plane and the longitudinal direction of the needle were set to $\boldsymbol{x}_3'$ [23, 39]. We then calculated the orientation-dependent Eshelby's tensor and the elastic energy increment by changing the rotation angle $(\phi,\ \psi)$ from 0° to 180° per 10° steps. The original coordinate system with $(\phi,\ \psi) = (0°, 0°)$ was set as $\boldsymbol{x_1}-\boldsymbol{x_2}-\boldsymbol{x_3} = [111]_\beta-[11\bar{2}]_\beta-[1\bar{1}0]_\beta$. Considering the symmetry of the ellipsoids, we calculated the strain field in only the first quadrants of the $\boldsymbol{x_1'}-\boldsymbol{x_2'}$ and $\boldsymbol{x_1'}-\boldsymbol{x_3'}$ planes by setting the center of the ellipsoidal inclusion at the origin of the $\boldsymbol{x}'$ coordinate system. Note that determining a unit for the half axes is unnecessary because Eshelby's tensor is independent of the inclusion volume, and the positions in this study are unitless.

3.2 Results and discussion

Fig. 2 shows the calculated $\Delta E^{\mathrm{het}}(\phi, \psi)$ distribution of the ω and α precipitates for V, Nb and Ta additive species. Although the potential energy of the ω phase is higher than that of the β phase in Table 1 for V, we conducted Eshelby's ellipsoidal inclusion analysis because the energy difference is small. As shown in the figure, although the scale of ΔE^{het} map changes with respect to the additive species, the approximate shapes of the maps appear similar. This is because the nonzero components of eigenstrains in Table 3 are the same for all the additive species. For all the additive species, the disk shapes generally have smaller ΔE^{het} values than the needle shapes; however, the difference between the ΔE^{het} values of the disk and needle shapes is small for the ω precipitates. Except for V, the ω precipitates had a smaller ΔE^{het} than the α phase.

This is due to the small eigenstrains of the $\beta-\omega$ phase transformation. The minimum value of ΔE^{het} ($\Delta E^{\mathrm{het}}_{\mathrm{min}}$) is at $(\phi,\ \psi) = (20°, 80°)$ for the α phase of all additive species. $\Delta E^{\mathrm{het}}_{\mathrm{min}}$ is at $(\phi,\ \psi) = (150°, 150°)$ for V, at $(\phi,\ \psi) = (0°, 90°)$ for Nb, and at $(\phi,\ \psi) = (90°, 30°)$ for Ta ω precipitates. The α disk with $(\phi,\ \psi) = (20°,\ 80°)$ is approximately a $[111]_\beta$ normal disk, which is consistent with the experimental observations; the habit plane of the α precipitate is $\{344\}_\beta$ or $\{334\}_\beta$ [40–42]. Although $(\phi,\ \psi)$ of $\Delta E^{\mathrm{het}}_{\mathrm{min}}$ are different with respect to the additive species for ω precipitates, considering the ΔE^{het} is relatively small in any $(\phi,\ \psi)$ and shapes (disk and needles) compared with α phase and the rough shape of ΔE^{het} maps is similar, we think a good interpretation is that ω can take various shapes and orientations because of its small eigenstrains.

Table 4 lists the data for $\Delta E^{\mathrm{het}}_{\mathrm{min}}$ and $\Delta E_{\mathrm{total}}$. For V addition, the stability of ω precipitates is lower than that of the β matrix, whereas the stability of α precipitates is higher than that of the β matrix; nonetheless, the energy difference between β and α decreases. Thus, α phases are the most stable, even if one takes into account the elastic energy increment due to the heterogeneity of α secondary phases. This is consistent with the experimental observations which indicate the presence of α precipitates in V additive titanium alloys after aging, which are transformed from the initial ω precipitates [14]. For Nb addition, DFT calculations indicated that the ω and α phases were more stable than the β phases. However, from the marginally positive $\Delta E_{\mathrm{total}}$ values, we confirmed that the β matrix was the most stable, and the ω and α precipitates were less stable than the β matrix (or equally stable). This demonstrates that the energy hierarchy of the α, β and ω phases, calculated using DFT atomistic simulations, may be altered when the effects of heterogeneity are considered. Thus, at high Nb concentrations, our results suggest that the secondary phase in the β matrix is prevented. However, at relatively low Nb concentrations, the secondary ω or α phases may nucleate because they are more stable than the β phases of pure Ti. For Ta addition, the results suggest that the ω precipitates were the most stable. This is because the ΔE_{DFT} of ω in Table 1 is considerably small. However, the α precipitates in this case may not be nuclear because $\Delta E_{\mathrm{total}}$ of α is higher than that of ω.

In the discussion above, we focused primarily on the ω and α precipitates in β matrix. However, considering that the order of phase transformation is β to ω to α, a coexistence of the three phases is also possible: ω nucleates in the β matrix, then α nucleates in the ω *intermediate* matrix, and the ω precipitate remains in the β matrix. We now investigate the stability of this situation. The intermediate ω phase can be considered as a matrix distorted by the original β matrix. Considering the calculated elastic strain $\varepsilon^{\mathrm{inc}}_{ij} - \epsilon^{\mathrm{inc}}_{ij}$ for the ω precipitates with $\Delta E^{\mathrm{het}}_{\mathrm{min}}$ as the external strain $\varepsilon^{\mathrm{ex}}_{ij}$, we applied the same Eshelby's ellipsoidal inclusion analysis to α precipitates in ω matrix. Fig. 3 shows the calculated ΔE^{het} map. Similar to the above results, the disk shapes are energetically favorable and $\Delta E^{\mathrm{het}}_{\mathrm{min}}$ is at $(\phi,$

$\psi) = (20°, 90°)$ for the V additive, and at $(\phi,\ \psi) = (140°, 80°)$ for the Nb and Ta additives. The $(\phi,\ \psi)$ value of $\Delta E_{\min}^{\text{het}}$ is almost the same as that of α disk in β matrix for V though $(\phi,\ \psi)$ of $\Delta E_{\min}^{\text{het}}$ is different from that for Nb and Ta additives. However, because ΔE^{het} values at $(\phi,\ \psi) = (20°, 90°)$ for Nb and Ta are almost same as those at $(\phi,\ \psi) = (140°, 80°)$, we think the orientation $(\phi,\ \psi) = (20°, 90°)$ is also possible for Nb and Ta. Interestingly, for the Nb and Ta additives, although the value of $\Delta E_{\min}^{\text{het}}$ is positive for the α precipitates in β matrix, the value of $\Delta E_{\min}^{\text{het}}$ is negative in this case. This means that the $\omega-\alpha$ phase transformation in the intermediate ω matrix and the coexistence of the three phases are elastically favored. This is because the elastic strains due to the α precipitation neutralized the external strain $\varepsilon_{ij}^{\text{ex}}$ in the ω intermediate matrix due to the β matrix. Using the above results, we calculated ΔE_{total} as

$$\Delta E_{\text{total}} = \Delta E_{\text{DFT}}(\omega) + V_{\text{atom}}(\Delta E_{\min}^{\text{het}}(\omega \text{ in } \beta) + \Delta E_{\min}^{\text{het}}(\alpha \text{ in } \omega)),$$

for the coexistence of the three phases. The values of ΔE_{total} are listed in Table 4. The results suggest that stable precipitates in the β matrix does not change for the V additive as α phase. Moreover, if the ω phase exists in the β matrix, the coexistence of the three phases is favored for the Nb additive owing to the negative $\Delta E_{\min}^{\text{het}}$ (however, we note that the ω precipitate itself is less stable than the β matrix). For the Ta additive, ω precipitates were favored despite the negative $\Delta E_{\min}^{\text{het}}$ because ΔE_{DFT} in Table 1 is considerably low.

Finally, the calculated strain field around the α disk in the β matrix for the V additive is shown in Fig. 4 and that around the ω disk for the Nb and Ta additives is shown in Fig. 5. We calculated the strain fields for 50 discrete positions at even intervals in the range from 0 to 25 for $\boldsymbol{x_1'}$ and $\boldsymbol{x_2'}$ and from 0 to 2 for $\boldsymbol{x_3'}$. The strain field maps were obtained after a linear interpolation. For the V additive, a large strain field with various strain components was observed. In particular, ε_{11} was quite large and approximately 0.1 near the precipitate. This can be attributed to the mixture of the eigenstrains of the $\beta-\omega$ and $\omega-\alpha$ phase transformations. This type of residual strain field may have both positive and negative effects on the mechanical properties of titanium alloys: for example, it may prevent the movement of dislocations (positive) or help the nucleation of cracks (negative). In contrast, only small shear components exist around the ω precipitates for the Nb and Ta additives. Thus, ω precipitates may not cause residual (internal) strain (or stress), and α precipitates may play a more important role than ω precipitates in precipitation strengthening.

Table 4: Potential energy differences ΔE_{total} of ω and α titanium precipitates from β titanium matrix for each additive element, calculated by considering the elastic energy increment due to the heterogeneity. The potential energies are in eV/atom. The $\Delta E_{\text{min}}^{\text{het}}$ (eV/nm^3) and V_{atom} (nm^3) data are also included.

		ω in β matrix		α in β matrix		α in ω matrix	
	V_{atom}	$\Delta E_{\text{min}}^{\text{het}}$	ΔE_{total}	$\Delta E_{\text{min}}^{\text{het}}$	ΔE_{total}	$\Delta E_{\text{min}}^{\text{het}}$	ΔE_{total}
Ti_5V_1	0.0995	0.8127	0.0159	0.7423	-0.0012	3.5881	0.0059
Ti_5Nb_1	0.1043	0.5588	0.0050	0.9611	0.0077	-1.2454	-0.0207
Ti_5Ta_1	0.1046	0.0094	-0.0365	0.0136	-0.0136	-1.0656	-0.0358

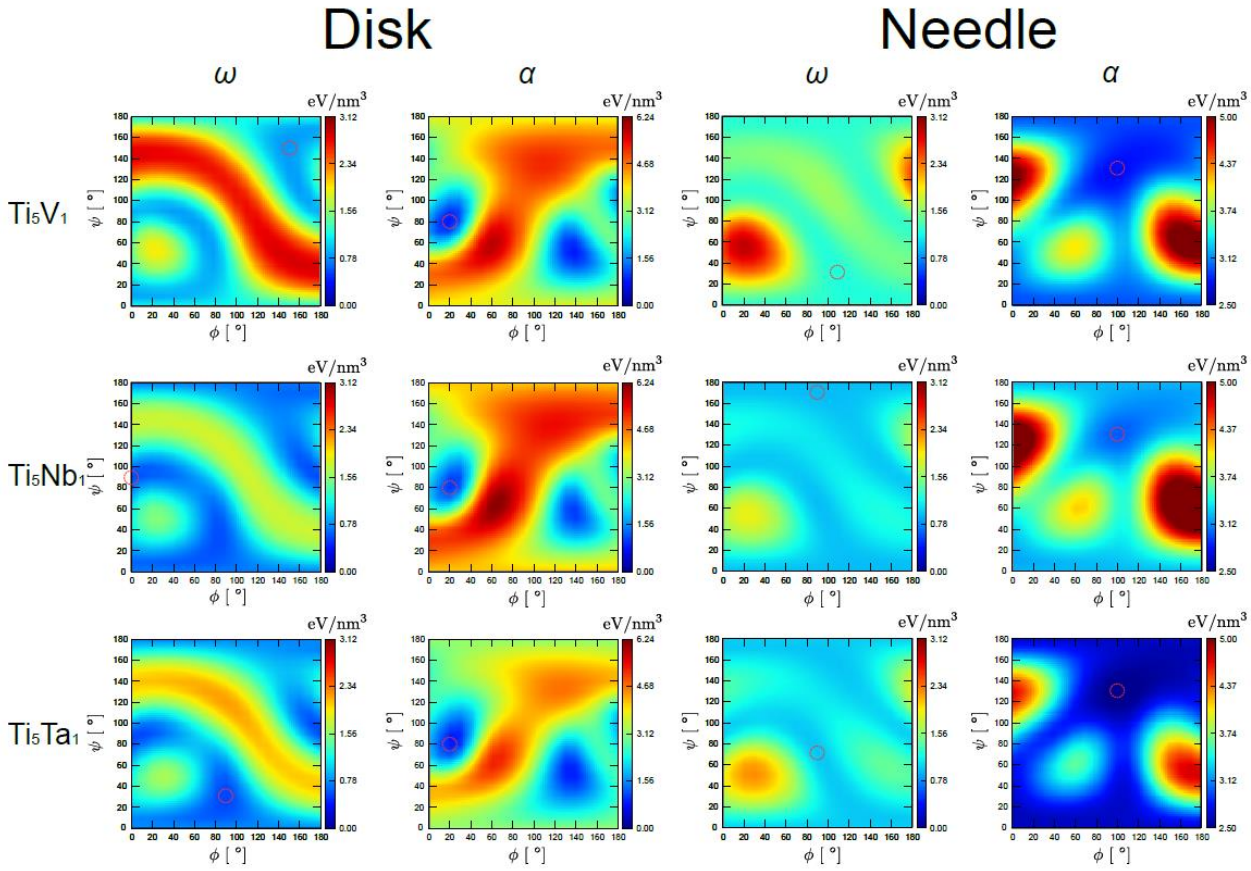

Figure 2: Change in elastic energy increment ΔE^{het} with respect to ϕ and ψ for V, Nb, and Ta additive: ω and α titanium precipitates in β titanium matrix. Broken circle indicates the area with the minimum ΔE^{het} ($\Delta E_{\text{min}}^{\text{het}}$).

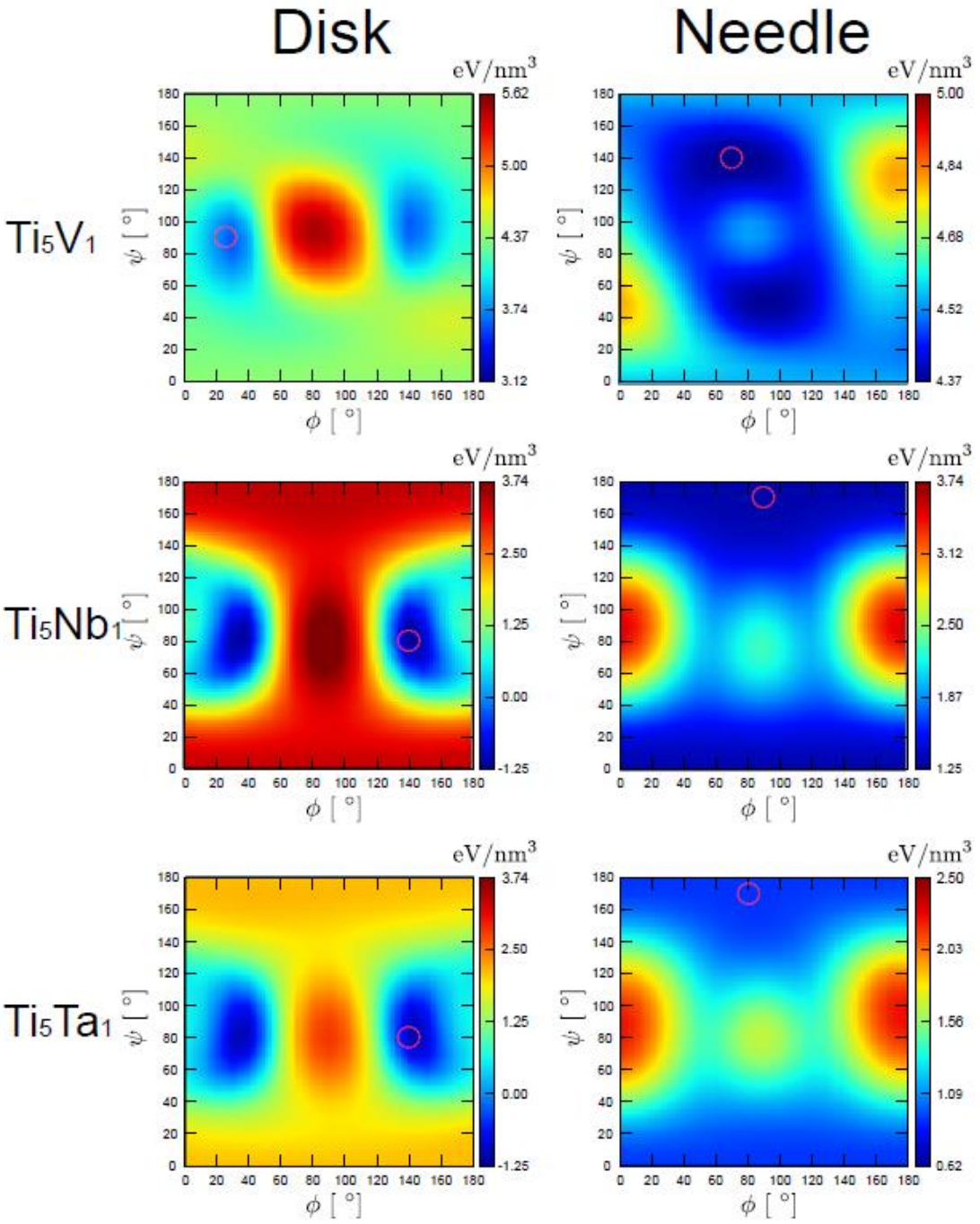

Figure 3: Change in elastic energy increment ΔE^{het} with respect to ϕ and ψ for V, Nb, and Ta additive: α titanium precipitates in ω titanium intermediate matrix. Broken circle indicates the area with the minimum ΔE^{het} ($\Delta E^{\mathrm{het}}_{\mathrm{min}}$).

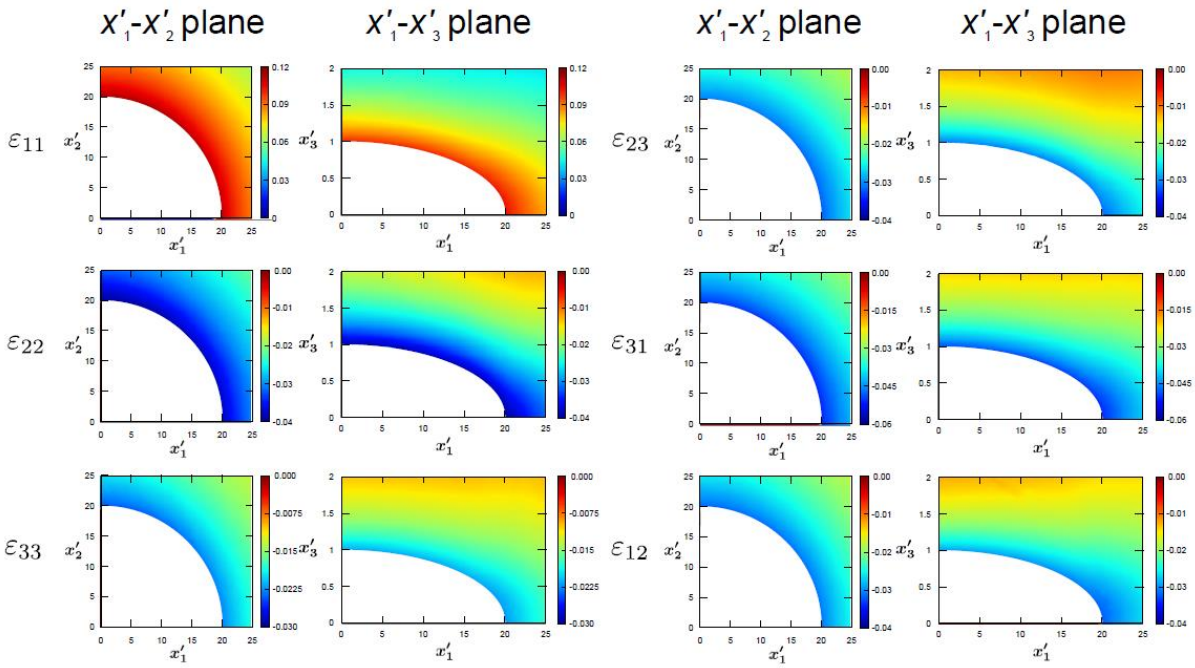

Figure 4: Strain fields around $(\phi,\ \psi) = (20°, 80°)$ α disk of Ti_5V_1 on the first quadrant of $\boldsymbol{x_1'}-\boldsymbol{x_2'}$ and $\boldsymbol{x_1'}-\boldsymbol{x_3'}$ planes. Note that all strain components are described in the original coordinate system $\boldsymbol{x_1}-\boldsymbol{x_2}-\boldsymbol{x_3} = [111]_\beta - [11\bar{2}]_\beta - [1\bar{1}0]_\beta$ and the strain fields inside the ellipsoid were omitted.

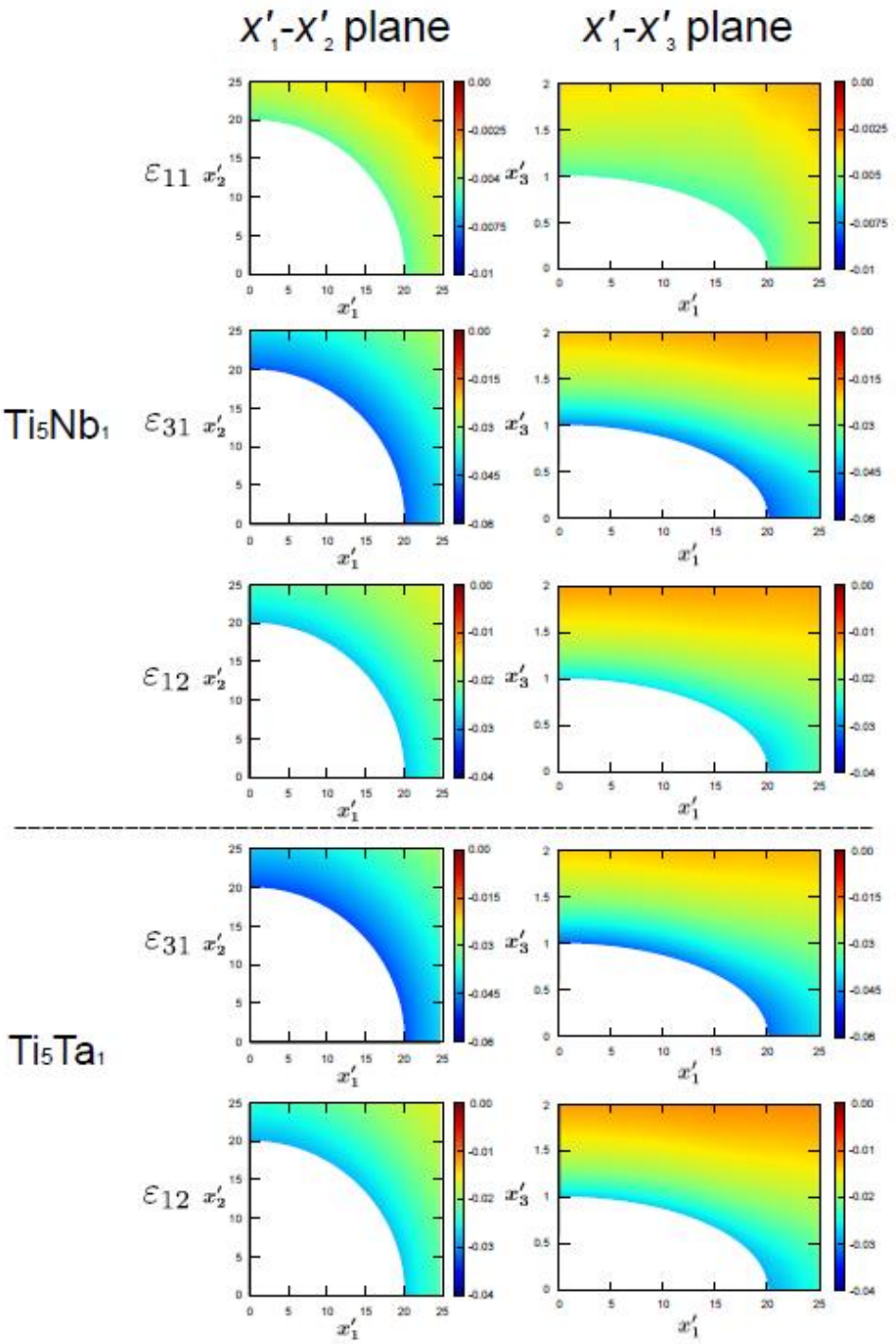

Figure 5: Strain fields around $(\phi,\ \psi) = (0°, 90°)$ ω disk of $Ti_5Nb_1$and $(\phi,\ \psi) = (90°, 30°)$ ω disk of Ti_5Ta_1 on the first quadrant of $\boldsymbol{x_1'}-\boldsymbol{x_2'}$ and $\boldsymbol{x_1'}-\boldsymbol{x_3'}$ planes. Note that all strain components are described in the original coordinate system $\boldsymbol{x_1}-\boldsymbol{x_2}-\boldsymbol{x_3} = [111]_\beta-[11\bar{2}]_\beta-[1\bar{1}0]_\beta$. The magnitudes of the strain fields of other strain components that are not shown in this figure are extremely small (lower than 10^{-3}) and we believe that they are ignorable. The strain fields inside the ellipsoid were omitted.

4. Summary

In summary, we combined DFT atomistic simulations and Eshelby's ellipsoidal inclusion analysis for the $ab\ initio$ energetical prediction of the phase stability of β titanium alloys with Mo, V, W, Nb, and Ta additives as β stabilizer elements. In particular, we accounted for the heterogeneity of the secondary ω and α phases (precipitation) in β matrix. For all β stabilizer species, apart from significant energetic stabilization of the β phase, significant elastic stabilization was observed. The addition of Mo and W turned the β phase the most energetically stable; secondary ω and α precipitates may hardly nucleate in β phase in high concentration condition. Although the V, Nb, and Ta additives stabilize β phase significantly, the β phase remains metastable. V and Ta respectively helped the precipitation of α and ω. For Nb addition, the possibility of a coexistence of ω and α in the β matrix was suggested. The strain fields around the precipitates were also investigated, and the results suggested that α precipitates cause a large residual strain around them, whereas ω precipitates do not. The phase stability depends strongly on the concentration of the additives even when the same additive element is used. Hence, we intend to investigate the phase stability of β titanium alloys with lower concentrations of β stabilizer elements in future work.

Acknowledgements

This study was partially supported by JSPS KAKENHI (Grant Number JP21K03771)

References

[1] R. R. Boyer, Attributes, characteristics, and applications of titanium and its alloys, JOM 62 (2010) 21-24.

[2] S. Liang, Review of the Design of Titanium Alloys with Low Elastic Modulus as Implant Materials, Adv. Eng. Mater. 22 (2020) 2000555.

[3] P. J. Bania, Beta titanium alloys and their role in the titanium industry, JOM 46 (1994) 16-19.

[4] R. Boyer, R. Briggs, The use of Titanium Alloys in the Aerospace Industry, J. Mater. Eng. Perform. 14 (2005) 681–685.

[5] S. Nyakana, J. Fanning, R. Boyer, Quick Reference Guide for β Titanium Alloys in the 00s, J. Mater. Eng. Perform. 14 (2005) 799–811.

[6] R. G. Hennig, D. R. Trinkle, J. Bouchet, S. G. Srinivasan, R. C. Albers, J. W. Wilkins, Impurities block the α to ω martensitic transformation in titanium, Nature Mater. 4 (2005) 129–133.

[7] M. Niinomi, M. Nakai, J. Hieda, Development of new metallic alloys for biomedical applications, Acta Biomater. 8 (2012) 3888–3903.

[8] M. Morinaga, N. Yukawa, H. Adachi, Theory of the *d* Electrons Alloy Design, Tetsu-to-Hagane 71 (1985) 1441–1451.

[9] D. Kuroda, M. Niinomi, M. Morinaga, Y. Kato, T. Yashiro, Design and mechanical properties of new type β titanium alloys for implant materials, Mater. Sci. Eng. A 243 (1998) 244–249.

[10] Y. Ohmori, T. Ogo, K. Nakai, S. Kobayashi, Effects of ω-phase precipitation on $\beta\rightarrow\ \alpha$, α'' transformations in a metastable titanium alloy, Mater. Sci. Eng. A 312 (2001) 182–188.

[11] T. Li, D. Kent, G. Sha, M. S. Dargusch, J. M. Cairney, The mechanism of ω-assisted α phase formation in near β-Ti alloys, Scr. Mater. 104 (2015) 75–78.

[12] T. Li, D. Kent, G. Sha, L. T. Stephenson, A. V. Ceguerra, S. P. Ringer, M. S. Dargusch, J. M. Cairney, New insights into the phase transforma-tions to isothermal ω and ω-assisted in near β-Ti alloys, Acta Mater.106 (2016) 353–366.

[13] Y. Zheng, R. E. Williams, D.Wang, R. Shi, S. Nag, P. Kami, J. M. Sosa, R. Banerjee, Y. Wang, H. L. Fraser, Role of ω phase in the formation of extremely refined intragranular α precipitates in metastable β-titanium alloys, Acta Mater. 103 (2016) 850–858.

[14] A. Devaraj, V. V. Joshi, A. Srivastava, S. Manandhar, V. Moxson, V. A. Duz, C. Lavender, A low-cost hierarchical nanostructured beta-titanium alloy with high strength, Nature Comm. 7 (2016) 11176.

[15] A. Jain, S. P. Ong, G. Hautier, W. Chen, W. D. Richards, S. Dacek, S. Cholia, D. Gunter, D. Skinner, G. Ceder, et al., Commentary: The materials project: A materials genome approach to accelerating materials innovation, APL mater. 1 (2013) 011002.

[16] M. De Jong, W. Chen, T. Angsten, A. Jain, R. Notestine, A. Gamst, M. Sluiter, C. K. Ande, S. Van Der Zwaag, J. J. Plata, et al., Charting the complete elastic properties of inorganic crystalline compounds, Sci. data 2 (2015) 1–13.

[17] S. Z. Han, E. A. Choi, S. H. Lim, S. Kim, J. Lee, Alloy design strategies to increase strength and its trade-offs together, Prog. Mater. Sci. 117 (2021) 100720.

[18] D. R. Trinkle, R. G. Hennig, S. G. Srinivasan, D. M. Hatch, M. D. Jones, H. T. Stokes, R. C. Albers, J. W. Wilkins, New Mechanism for the α to ω Martensitic Transformation in Pure Titanium, Phys. Rev. Lett. 91 (2003) 025701.

[19] H. Ikehata, N. Nagasako, T. Furuta, A. Fukumoto, K. Miwa, T. Saito, First-principles calculations for development of low elastic modulus Ti alloys, Phys. Rev. B 70 (2004) 174113.

[20] D. Raabe, B. Sander, M. Friák, D. Ma, J. Neugebauer, Theory-guided bottom-up design of β-titanium alloys as biomaterials based on first principles calculations: Theory and experiments, Acta Mater. 55 (2007) 4475–4487.

[21] K. Shitara, K. Yokota, M. Yoshiya, J. Umeda, K. Kondoh, First-principles design and experimental validation of β-Ti alloys with high solid-solution strengthening and low elasticities, Mater. Sci. Eng. A 843(2022) 143053.

[22] X. Fu, X. D. Wang, B. Zhao, Q. Zhang, S. Sun, J. J. Wang, W. Zhang, L. Gu, Y. Zhang, W. Z. Zhang, W. Wen, Z. Zhang, L. Qing Chen, Q. Yu, E. Ma, Atomic-scale observation of non-classical

nucleation-mediated phase transformation in a titanium alloy, Nature Mater. 21 (2022) 290–296.
[23] A. Ishii, *Ab initio* morphology prediction of Zr hydride precipitates using atomistically informed Eshelby's ellipsoidal inclusion, Comput. Mater.Sci. 211 (2022) 111500.
[24] A. Ishii, Elastic investigation for the existence of B33 phase in TiNi shape memory alloys using atomistically informed Eshelby's ellipsoidal inclusion, Comput. Mater. Sci. 218 (2023) 111954.
[25] A. Ishii, *Ab initio* prediction of temperature-dependent stability of heterogeneous B19' phase in TiNi alloy using atomistically informed Eshelby's ellipsoidal inclusion, Mater. Today Comm. 35 (2023) 105861.
[26] A. Ishii, Morphology prediction of elastically interacting Zr hydride precipitates and cracks in α-Zr using atomistically informed Eshelby's ellipsoidal inclusion, Comput. Mater. Sci. 231 (2024) 112568.
[27] M. Tane, H. Nishio, D. Egusa, T. Sasaki, E. Abe, E. Miyoshi, S. Higashino, Effects of aluminum and oxygen additions on quenched-in compositional fluctuations, dynamic atomic shuffling, and their resultant diffusionless isothermal ω transformation in ternary Ti-V-based alloys with bcc structure, Acta Mater. 255 (2023) 119034.
[28] A. Rabinkin, M. Talianker, O. Botstein, Crystallography and a model of the $\alpha \rightarrow \omega$ phase transformation in zirconium, Acta Metall. 29 (1981) 691–698.
[29] G. Kresse, J. Furthmüller, Efficient iterative schemes for ab initio total-energy calculations using a plane-wave basis set., Physi. Rev. B 54 (1996) 11169–11186.
[30] G. Kresse, D. Joubert, From ultrasoft pseudopotentials to the projector augmented-wave method, Phys. Rev. B 59 (1999) 11–19.
[31] J. Perdew, K. Burke, M. Ernzerhof, Generalized Gradient Approximation Made Simple, Phys. Rev. Lett. 77 (1996) 3865–3868.
[32] M. Born, On the stability of crystal lattices. I, Math. Proc. Cambridge Philos. Soc. 36 (1940) 466–478.
[33] F. Mouhat, F.-X. Coudert, Necessary and sufficient elastic stability conditions in various crystal systems, Phys. Rev. B 90 (2014) 224104.
[34] T. Mura, Micromechanics of defects in solids, Springer Science & Business Media, 2013.
[35] J. D. Eshelby, The determination of the elastic field of an ellipsoidal inclusion, and related problems, Proceedings of the royal society of London. Series A. Mathematical and physical sciences 241 (1957) 376–396.
[36] J. D. Eshelby, Elastic inclusions and inhomogeneities, Prog. solid mech. 2 (1961) 89–140.
[37] N. Kinoshita, T. Mura, Elastic fields of inclusions in anisotropic media, Phys. Stat. Solidi (A) 5 (1971) 759–768.
[38] T. Mura, P. C. Cheng, The elastic field outside an ellipsoidal inclusion, J. Appl. Mech. 44 (1977) 591–594.

[39] M. Kato, T. Fujii, S. Onaka, Elastic strain energies of sphere, plate and needle inclusions, Mater. Sci. Eng. A 211 (1996) 95–103.

[40] Y. C. Liu, H. Margolin, Martensite Habit Plane in Quenched Ti-Mn Alloys, JOM 5 (1953) 667–670.

[41] S.Weinig, E. S. Machlin, Data for one of the martensitic transformations in an 11 pct Mo-Ti alloy, JOM 6 (1954) 1280–1281.

[42] P. Gaunt, J. W. Christian, The crystallography of the $\beta - \alpha$ transformation in zirconium and in two titanium-molybdenum alloys, Acta Metall. 7 (1959) 534–543.